Spin Waves in Nickel Nanorings of Large Aspect Ratio

Z. K. Wang, H. S. Lim, H. Y. Liu, S. C. Ng, and M. H. Kuok*
Department of Physics, National University of Singapore, Singapore 117542, Singapore

L. L. Tay and D. J. Lockwood
Institute for Microstructural Sciences, National Research Council, Ottawa, K1A 0R6, Canada

M. G. Cottam
Department of Physics and Astronomy, University of Western Ontario, London, Ontario N6A 3K7, Canada

K. L. Hobbs, P. R. Larson, J. C. Keay, G. D. Lian, and M. B. Johnson
Department of Physics and Astronomy, University of Oklahoma, Oklahoma 73019, USA
(Received 26 October 2004; published 7 April 2005)

The spin dynamics of high-aspect-ratio nickel nanorings in a longitudinal magnetic field have been investigated by Brillouin spectroscopy and the results are compared with a macroscopic theory and three-dimensional micromagnetic simulations. Good agreement is found between the measured and calculated magnetic field dependence of the spin wave frequency. Simulations show that as the field decreases from saturation, the rings switch from a ''bamboo'' to a novel ''twisted bamboo'' state at a certain critical field, and predict a corresponding dip in the dependence of the spin wave frequency on the magnetic field.

DOI: 10.1103/PhysRevLett.94.137208 PACS numbers: 75.10.Jm, 75.30.Ds, 75.75.+a, 78.35.+c

Patterned magnetic nanostructures, such as arrays of rings, dots, stripes, and wires, have been extensively investigated because of their potential applications in magnetic memory and sensing devices [1–7]. Magnetic nanorings, in particular, are excellent candidates for high-density storage devices because of the existence of vortex or flux-closed states in which the magnetization is oriented circularly and for which stray magnetic fields are essentially absent [8,9]. In their study of mesoscopic ring magnets, Rothman *et al*. [10] discovered the existence of a bidomain state which they termed the onion state. Extensive research has been carried out on the static properties of micron- and nanoscale ring magnets, mainly using the magneto-optical Kerr effect [8,10], anisotropic magnetoresistance [11] or local Hall effect techniques [12]. However, information on their dynamical properties is scarce. Thus far, a recent ferromagnetic resonance characterization undertaken by Xu *et al*. [13] is the only reported study of the dynamical properties of these ring magnets.

In this Letter we present findings of an investigation, by Brillouin light scattering, micromagnetic simulations, and a macroscopic theory, of the dynamical properties of nickel nanorings. Previously studied magnetic rings were flat, with heights (ranging from a few to tens of nanometers) much shorter than their outer diameters and their properties were investigated under an applied transverse (normal to ring axis) magnetic field. By contrast, the nanosize nickel rings investigated here have a height that is some 1.5 times longer than their outer diameter (≈ 100 nm) and the behavior of their spin waves in an applied *longitudinal* (parallel to ring axis) magnetic field was studied.

The nanoring array was fabricated using Ar^+ sputter redeposition of nickel in an anodic aluminum oxide (AAO) mask [14]. The AAO template was synthesized using a two-step anodization process described in detail elsewhere [15,16]. To start, the through-hole porous alumina template was used as an evaporation mask to define an array of nickel dots. This was followed by an ion etching step that left behind sputter redeposited nickel dot material around the pore walls. Removal of the AAO template yielded a hexagonal array of nickel nanorings as shown in Fig. 1. The periodic spacing of the array is 105 nm and the rings have an inner diameter of 65 nm, a wall thickness of 15 nm, and a height of 150 nm.

Brillouin measurements were performed at room temperature in the 180 °-backscattering geometry using a (3 + 3)-pass tandem Fabry-Perot interferometer equipped with a silicon avalanche diode detector, and 40 mW of the

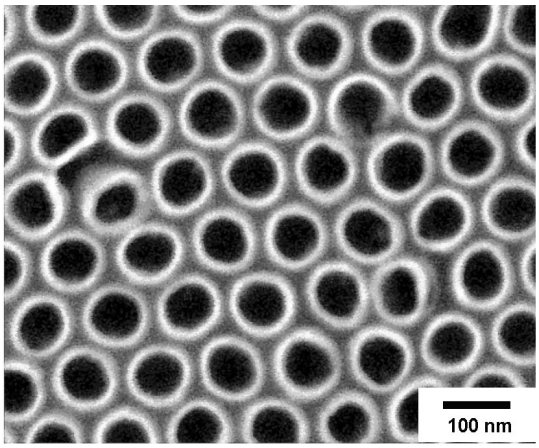

FIG. 1. Scanning electron microscope micrograph of the hexagonal array of the high-aspect-ratio nickel nanorings.

514.5 nm line of an argon-ion laser for excitation. A continuous stream of pure argon gas was directed at the irradiated spot on the sample surface to cool it and to keep air away from it. In the scattering configurations employed, the symmetry axes of the nanorings were aligned parallel (longitudinal) to the applied static magnetic field, which was generated by a computer-controlled electromagnet. Prior to the start of the measurements, the sample was saturated in a 1.0 T field directed parallel to the symmetry axes of the rings. Spectra were recorded in *p-s* polarization with an average scanning duration of 10 h.

The time evolution of the magnetization $\boldsymbol{M}$ of a magnetic system can be obtained by integrating the Landau-Lifshitz equation,

$$\frac{d\boldsymbol{M}}{dt} = \gamma \boldsymbol{M} \times \boldsymbol{H}_{\text{eff}} + \frac{\gamma\alpha}{M_S} \boldsymbol{M} \times (\boldsymbol{M} \times \boldsymbol{H}_{\text{eff}}),$$

where $\boldsymbol{H}_{\text{eff}}$ is the effective field [17], γ the gyromagnetic ratio, and α the damping coefficient. The equilibrium magnetization configuration, corresponding to an energy minimum for each applied field, was determined by micromagnetic simulations, using the OOMMF three-dimensional (3D) package [18]. Since the Ni rings are amorphous, the magnetocrystalline anisotropy constant was set to zero. The material parameters used in the simulations are the saturation magnetization $M_S = 480 \times 10^3$ A/m, exchange stiffness constant $A = 10 \times 10^{-12}$ J/m, and $\gamma = 194.4$ GHz/T [19]. In our 3D computations, a discretization cell of dimensions $3 \times 3 \times 15$ nm^3 was used with α set to a value of 0.3. This value of α was chosen so that the equilibrium magnetization state can be obtained in a reasonable time. Smaller values have also been used but all lead to the same equilibrium state.

The magnetization distributions within our high-aspect-ratio nanoring were theoretically determined at various longitudinally applied magnetic fields. Our simulations show that under strong fields the spins are aligned along the field direction (i.e., parallel to the symmetry axis of the rings) corresponding to what we call the "bamboo" state. Below a certain critical field, the rings switch to another state. An interesting feature of this state is the opposite circulation of the component of spins in the top and bottom planes normal to the ring axis, while in the middle planes the spins are essentially parallel to the ring axis. For this reason we term this state the "twisted bamboo" state. Magnetization distributions of this state, simulated at an applied field H_0 of 5 mT, for various cross sections either containing or normal to the ring axis are illustrated in Fig. 2. Confirmation of this switching behavior within a microscopic modeling approach is found by extending the calculations of Nguyen and Cottam [20] for nanowires.

We also evaluated the frequencies of spin waves (SWs) in the nanorings using the following micromagnetic approach. After the equilibrium magnetization configuration

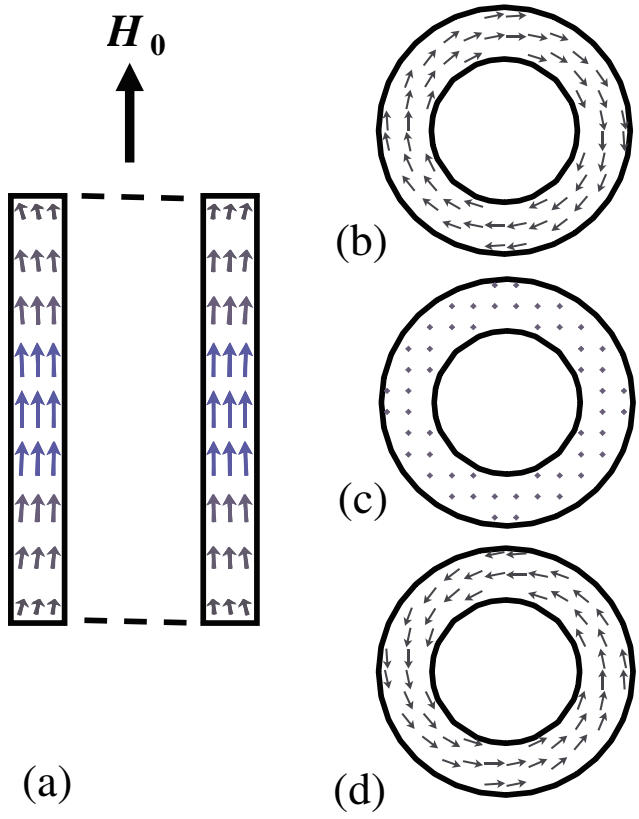

FIG. 2 (color online). Simulated magnetization distributions ($H_0 = 5$ mT) for a nickel nanoring in the twisted bamboo phase. (a) A cross section containing the ring axis, and (b) top, (c) middle, and (d) bottom cross sections normal to the ring axis (viewed along the $-\boldsymbol{H}_0$ direction).

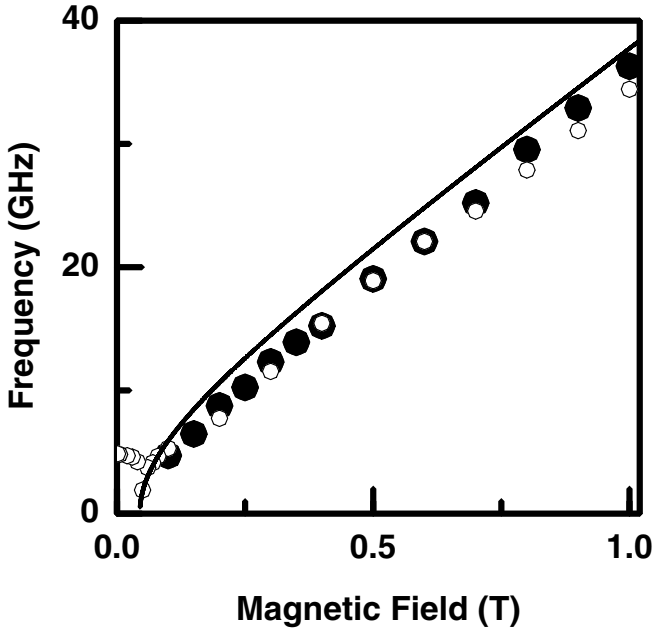

FIG. 3. Magnetic field dependence of the frequencies of spin waves in a nickel nanoring. Measured frequencies are represented by closed circles, while calculated ones by open circles (micromagnetic simulations) and a solid curve (analytical equation $\omega = \gamma[H_i\{4\pi M_S + H_i\}]^{1/2}$).

has been determined, as described above, the relaxed structure was used as the input in the subsequent calculation in which α was set to 0.000 001 and the corresponding SW frequency was obtained from a Fourier transform of the magnetization $\boldsymbol{M}$. The calculated variation with magnetic field of the SW frequency is presented in Fig. 3 which reveals that the frequency is strongly dependent on the field and the presence of a dip in the vicinity of a critical field at about 50 mT. Note that a qualitatively similar dip could in principle occur for a uniformly magnetized ellipsoid if the field is not applied along its easy axis. However, the situation is different here since the dip is predicted by our micromagnetic simulations for a nanoring with the field set exactly along its easy axis. Our chosen cell size of $3 \times 3 \times 15$ nm^3 was found to be sufficiently small as computations based on a $3 \times 3 \times 3$ nm^3 cell size produced results close to those of the chosen size. For example, for an applied field of 1.0 T, the respective cell sizes yielded SW frequencies of 34.4 and 34.5 GHz, and both cells yielded 18.9 GHz for a field of 0.5 T.

Figure 4 shows a typical *p-s* polarized Brillouin spectrum, recorded at an incident angle of 60 °, of the nanoring sample in a 0.8 T field. The spectral peaks were fitted with a Lorentzian function, as shown in Fig. 4, and the measured variation of the SW frequency with applied field is displayed in Fig. 3. Elastic scattering precluded the measurement of SW frequencies below ≈ 5 GHz (corresponding to 0.1 T applied field) and hence the predicted dip in the field dependence of the frequency eluded observation. However, over the frequency range measured, the excellent agreement between theory and experiment (see Fig. 3) lends credence to our simulation procedure for the evaluation of SW frequencies.

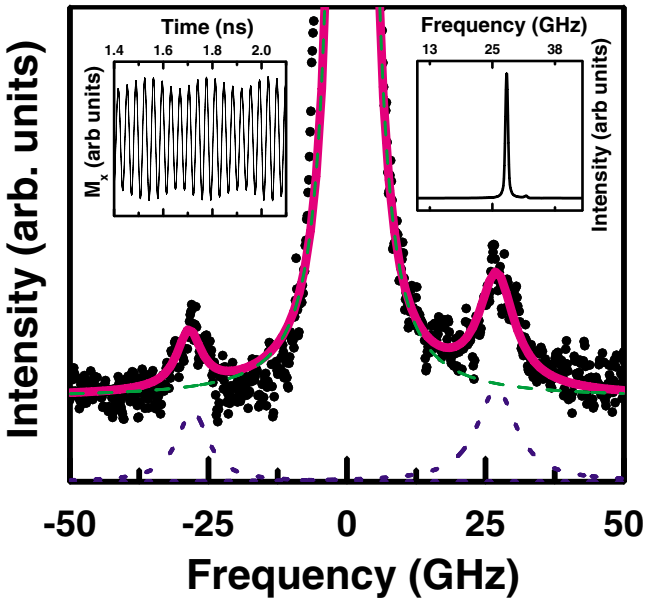

FIG. 4 (color online). Brillouin spectrum of a nickel nanoring array in a 0.8 T magnetic field applied parallel to the symmetry axis of the rings. Experimental data are denoted by dots. The spectrum is fitted with a Lorentzian function (dotted curve) and a background (dashed curve), and the resulting fitted spectrum is displayed as a solid curve. Left inset: Simulated time dependence of the transverse magnetization component of the spin wave at $H_0 = 0.8$ T. Right inset: Corresponding spin wave frequency obtained via a Fourier transform.

The Zeeman, demagnetization and exchange contributions to the total energy of the ring, as a function of applied magnetic field, have been calculated and results are shown in Fig. 5. At high applied fields, the Zeeman contribution predominates and the magnetization configuration is such that the spins are essentially aligned along the applied field direction. Additionally, this parallel arrangement minimizes the exchange contribution to the total magnetic energy of the ring. Hence, the stable magnetization configuration is one where the spins are aligned parallel to the ring axis, corresponding to the bamboo state. Lowering of the field results in a reduction in the Zeeman contribution and as a consequence the other contributions become increasingly significant. In particular, the magnetization assumes a configuration in which the stray field, and hence, the demagnetization energy, is minimal. Thus, when the applied field is sufficiently low (depending on the length-to-diameter aspect ratio of the sample), the twisted bamboo state would result.

The Brillouin data were also analyzed based on a similar generalization of the Arias-Mills macroscopic dipole-exchange theory [21] that was used for the zero-field case for nickel nanowires [2]. In this theory, the SW frequencies for the ring can be expressed as

$$\omega = \gamma[Dq^2\{Dq^2 + 4\pi M_s + 2Dk^2\} + \{Dk^2\}^2 + H_t\{H_t + 2Dq^2 + 2Dk^2\} + 4\pi M_S H_t\{q^2/(q^2 + k^2)\}]^{1/2}. \quad (1)$$

Here k, which is determined by our scattering geometry, is

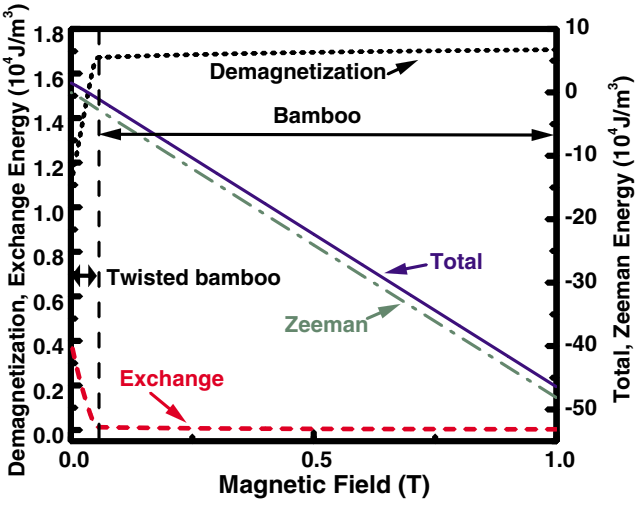

FIG. 5 (color online). Calculated Zeeman, demagnetization, and exchange contributions to the total energy of a nickel nanoring as a function of longitudinally applied magnetic field.

the component of the SW wave vector along the ring axis and q is an effective radial wave vector (as in [2]). The quantization condition for q is more complicated than assumed in [2] for the nickel nanowires, because the nanorings have both inner and outer surfaces where boundary conditions apply. When the wall thickness is relatively small, as in our experiments, there is a simplification and we may assume approximately that $q = n\pi/(R_2 - R_1)$ with $n \approx 0, 1, 2, \ldots$, where R_2 and R_1 are the respective outer and inner radii. A simple physical interpretation of this result is that it corresponds to fitting an (approximately) integer number n of half wavelengths into the wall thickness. The SW amplitudes also have an angular dependence like $\exp(im\theta)$, as in [2], where m is an integer, but the effect on q can be ignored when the wall thickness is small. Also in Eq. (1) the exchange term is $D = 2A/M_S$ and the effective longitudinal field is $H_t = H_0 - H_d$, which is positive for the bamboo phase. H_0 is the applied field and the demagnetizing field $H_d = 4\pi N_Z^{\mathrm{Ring}} M_S$ where N_Z^{Ring} is the demagnetizing factor.

For the very small k values ($\sim 10^{-7}$ m^{-1}) in the experiments, the above expression for ω simplifies considerably, since we have $k^2 \ll q^2$. This is quite possibly true even for the lowest SW mode, which corresponds to an effective n that is actually nonzero, although close to zero, depending on the surface pinning parameters. If we assume this inequality to apply then the frequency of this lowest mode can be approximated as $\omega = \gamma[H_t\{4\pi M_S + H_t\}]^{1/2}$. Using the expression formulated by Sato and Ishii [22] for N_Z^{Ring} of a finite cylinder, H_d was found to be about 35 mT, which is close to the simulated critical field value of 50 mT mentioned above. Calculated values of ω, based on the simplified expression, were found to agree well with measured and simulated values (see Fig. 3).

In conclusion, we have reported the first observation, by Brillouin light scattering, of the longitudinal magnetic field dependence of SWs in a nickel nanoring. Three-dimensional micromagnetic simulations and macroscopic calculations have also been performed for our high-aspect ratio nanorings. The measured magnetic field dependence of the SW frequency is in good agreement with the simulated and calculated results. Simulations revealed that under high magnetic fields, the rings assume a single-domain state, where the spins are aligned parallel to the symmetry axis of the rings, which we term the bamboo state. Additionally, at a critical field of 50 mT (related to the length of the sample) the rings switch to a novel twisted bamboo state characterized by the opposite circulation of the spin components in the top and bottom planes of the rings. This transition is manifested as a dip in the simulated magnetic field dependence of the SW frequency at about 50 mT.

This research was funded by the Agency for Science, Technology and Research (A*STAR) Singapore, the National Research Council of Canada, NSERC of Canada, and NSF of USA (grants no. DMR-0080054 and no. EPS-0132534).

*Corresponding author.
Electronic address: phykmh@nus.edu.sg

[1] H. Zheng, J. Wang, S. E. Lofland, Z. Ma, L. Mohaddes-Ardabili, T. Zhao, L. Salamanca-Riba, S. R. Shinde, S. B. Ogale, F. Bai, D. Viehland, Y. Jia, D. G. Schlom, M. Wuttig, A. Roytburd, and R. Ramesh, Science **303**, 661 (2004).
[2] Z. K. Wang, M. H. Kuok, S. C. Ng, D. J. Lockwood, M. G. Cottam, K. Nielsch, R. B. Wehrspohn, and U. Gösele, Phys. Rev. Lett. **89**, 027201 (2002).
[3] S. I. Kiselev, J. C. Sankey, I. N. Krivorotov, N. C. Emley, R. J. Schoelkopf, R. A. Buhrman, and D. C. Ralph, Nature (London) **425**, 380 (2003).
[4] M. Bailleul, D. Olligs, and C. Fermon, Phys. Rev. Lett. **91**, 137204 (2003).
[5] J. Jorzick, S. O. Demokritov, B. Hillebrands, M. Bailleul, C. Fermon, K. Y. Guslienko, A. N. Slavin, D. V. Berkov, and N. L. Gorn, Phys. Rev. Lett. **88**, 047204 (2002).
[6] M. Natali, I. L. Prejbeanu, A. Lebib, L. D. Buda, K. Ounadjela, and Y. Chen, Phys. Rev. Lett. **88**, 157203 (2002).
[7] S. A. Wolf, D. D. Awschalom, R. A. Buhrman, J. M. Daughton, S. Von Molnár, M. L. Roukes, A. Y. Chtchelkanova, and D. M. Treger, Science **294**, 1488 (2001).
[8] S. P. Li, D. Peyrade, M. Natali, A. Lebib, Y. Chen, U. Ebels, L. D. Buda, and K. Ounadjela, Phys. Rev. Lett. **86**, 1102 (2001).
[9] F. J. Castaño, C. A. Ross, C. Frandsen, A. Eilez, D. Gil, H. I. Smith, M. Redjdal, and F. B. Humphrey, Phys. Rev. B **67**, 184425 (2003).
[10] J. Rothman, M. Kläui, L. Lopez-Diaz, C. A. F. Vaz, A. Bleloch, J. A. C. Bland, Z. Cui, and R. Speaks, Phys. Rev. Lett. **86**, 1098 (2001).
[11] M. Kläui, C. A. F. Vaz, J. Rothman, J. A. C. Bland, W. Wernsdorfer, G. Faini, and E. Cambril, Phys. Rev. Lett. **90**, 097202 (2003).
[12] M. Steiner and J. Nitta, Appl. Phys. Lett. **84**, 939 (2004).
[13] W. Xu, D. B. Watkins, L. E. Delong, K. Rivkin, J. B. Ketterson, and V. V. Metlushko, J. Appl. Phys. **95**, 6645 (2004).
[14] K. L. Hobbs, P. R. Larson, G. D. Lian, J. C. Keay, and M. B. Johnson, Nano Lett. **4**, 167 (2004).
[15] H. Masuda and K. Fukuda, Science **268**, 1466 (1995).
[16] A. P. Li, F. Müller, A. Birner, K. Nielsch, and U. Gösele, J. Appl. Phys. **84**, 6023 (1998).
[17] W. F. Brown, Jr., *Micromagnetics* (Krieger, New York, 1978).
[18] The OOMMF package is available at http://math.nist.gov/oommf.
[19] J. R. Sandercock and W. Wettling, J. Appl. Phys. **50**, 7784 (1979).
[20] M. T. Nguyen and M. G. Cottam, J. Magn. Magn. Mater. **272-276**, 1672 (2004).
[21] R. Arias and D. L. Mills, Phys. Rev. B **63**, 134439 (2001).
[22] M. Sato and Y. Ishii, J. Appl. Phys. **66**, 983 (1989).